ECOGRAPHY

Size matters in quantitative radar monitoring of animal migration: estimating monitored volume from wingbeat frequency

Abstract:	Quantitative radar studies are an important component of studying the movement of birds. Whether a bird is detected or not depends upon its size, because the object size ultimately determines the monitored volume of a radar beam. Consequently, an accurate quantification of bird movements recorded by small-scale radar requires an accurate determination of the monitored volume for the objects in question, although this has tended to be ignored.
	Here, we demonstrate the importance of sensitivity settings for echo detection on the estimated movement intensities of different sized birds. The amount of energy reflected from a bird and detected by the radar receiver (echo size) depends not only on the bird's size and on the distance from the radar antenna, but also on the beam shape and the bird's position within this beam. We propose a method to estimate the size of a bird based on the wingbeat frequency, retrieved from the echo-signal, independent of the absolute echo size. The estimated bird-size allows calculation of size-specific monitored volumes, allowing accurate quantification of movement intensities. We further investigate the importance of applying size-specific monitored volume to quantify avian movements instead of using echo counts.
	We also highlight the importance of accounting for size-specific monitored volume of small scale radar systems, and the necessity of reporting technical information on radar parameters. Applying this framework will increase the quality and validity of quantitative radar monitoring.

Journal for submission: Ecography for ENRAM special issue

Running title: *RCS via WBF*

Title

Size matters in quantitative radar monitoring of animal migration: estimating monitored volume from wingbeat frequency

1   **Abstract**

2   Quantitative radar studies are an important component of studying the movement of birds.

3   <mark>Whether a bird is detected or not depends upon its size, because the object size ultimately</mark>

4   <mark>determines the monitored volume of a radar beam.</mark> Consequently, an accurate quantification of bird

5   movements recorded by small-scale radar requires an accurate determination of the monitored

6   volume for the objects in question, although this has tended to be ignored.

7   Here, we demonstrate the importance of sensitivity settings for echo detection on the estimated

8   movement intensities of different sized birds. The amount of energy reflected from a bird and

9   detected by the radar receiver (echo size) depends not only on the bird's size and on the distance

10   from the radar antenna, but also on the beam shape and the bird's position within this beam. We

11   propose a method to estimate the size of a bird based on the wingbeat frequency, retrieved from

12   the echo-signal, independent of the absolute echo size. The estimated bird-size allows calculation of

13   size-specific monitored volumes, allowing accurate quantification of movement intensities. We

14   further investigate the importance of applying size-specific monitored volume to quantify avian

15   movements instead of using echo counts.

16   We also highlight the importance of accounting for size-specific monitored volume of small scale

17   radar systems, and the necessity of reporting technical information on radar parameters. Applying

18   this framework will increase the quality and validity of quantitative radar monitoring.

19

20   **Keywords**

23

24   **Lexicon**

25   D_{max} [m]: Maximum distance (range) of detection. At D_{max}, the echo power received from an

26   object falls below the detection threshold $P_{r_{min}}$. D_{max} primarily depends on the object's RCS, and

27   radar properties such as the transmitted power P_t and antenna gain G_0 and wave length λ (*cf.* radar

28   equation in Lexicon, (Drake and Reynolds 2012) eq. 3.14b): $D_{max} = \sqrt[4]{\dfrac{P_t \cdot G_0{}^2 \cdot \lambda^2 \cdot RCS}{P_{r_{min}} \cdot (4 \cdot \pi)^3}}$

29   dB: The unit decibel expresses the logarithmic ratio on base 10 between the transmitted power (P_t)

30   and the received power (P_r). A proper calibration of the radar system allows expression of the power

31   in dBm, using a standard reference of 1 mW: $P_{r,dBm} = 10 \cdot \log_{10}(P_{r,W}/1_{mW})$

32   Echo signature: The echo intensity of an object varies during its transit of the radar beam. The echo

33   signature represents the temporal variation in echo intensity (*cf.* P_r in Lexicon). Fine scale temporal

34   variations in echo intensity are due to small changes in the object's aspect and reflectivity

35   properties.

36   Echo size [dBm]: Maximal echo intensity of an object as measured by the radar receiver (*cf.* P_r in

37   Lexicon) after removing low amplitude variations in echo intensity with a low pass filter. The echo

38   size depends on object properties (size, aspect, reflecting properties, etc.), radar properties (wave

39   length λ, transmitted power P_t, antenna gain G_0), the distance to the radar, and properties of the

40   atmosphere.

41   G_0 [dB]: The antenna gain is a measure which describes the extent to which the antenna directs the

42   beam towards the main beam axis (*sensu* Drake and Reynolds 2012).

43   λ [m]: Length of the electromagnetic waves, calculated as the speed of light (c, about $3 \cdot 10^8$ m * s^{-1})

44   divided by the emission frequency (f, e.g. 9.4 GHz): $\lambda = \frac{c}{f}$.

45   Mie region: The relationship between the object size and the RCS depends on the electromagnetic

46   wave length λ and can be described in three regions: optical region if object diameter >> λ, Mie

47   region if object diameter ≈ λ, Rayleigh region if object diameter << λ. The wave length of the 9.4 GHz

48   radar system used in this study is 3.2 cm (see Lexicon "wave length"). While the RCS of objects larger

49   than ten centimetres diameter is proportional to its size (optical region), the RCS of objects ranging

50   from one to ten centimetre is not proportional to the object size (Mie region) (see e.g. (Drake and

51   Reynolds 2012), p. 53). For instance, an object of 5 cm may produce an RCS of 25 cm^2 (5.64 cm

52   diameter), where as an object of 5.5 cm diameter may produce an RCS of 15 cm^2 (4.37 cm diameter).

53   This phenomenon progressively increases with decreasing object size, and is particularly strong for

3

54   objects between one to three centimetres with RCS up to four times the object size. In the Rayleigh

55   region, the decrease of RCS is steeper than the decrease of the object size.

56   Monitored volume: Also known as radar coverage or isoechoic contour, the monitoring volume

57   defines the maximal ranges for echo detection: the maximal detection distance D_{max}, as well as the

58   effective beam width (*cf.* $Width_{beam}$ in Lexicon). The monitored volume depends on the object size,

59   and increases with increasing object size.

60   MTR [bird * km^{-1} * h^{-1}]: Migration Traffic Rate is a standardised measure of bird movements (Lowery

61   1951, Liechti et al. 1995). It describes the number of birds crossing a virtual transect line of one

62   kilometre within one hour. By considering flight altitude, subsets can be given for different height

63   intervals. For example, the MTR of a period between t_1 and t_2 is the sum of the MTR-factors (s.

64   below) multiplied by the ratio between an hour and the time period [hour] between t_1 and t_2:

65   $MTR = \sum_{t_1 - t_2} MTR_{factor} \cdot \frac{1}{t_1 - t_2}$.

66   MTR_{factor}: The MTR-factor is defined as the ratio between the one kilometre transect line and the

67   effective beam width $Width_{beam}$, at the object's distance and for the object's estimated size:

68   $MTR_{factor} = 1000/Width_{beam}$. For example, MTR_{factor} equals five for a 200 m $Width_{beam}$. The

69   MTR-factor indicates the individual contribution of each echo to the MTR: e.g. the sum of all MTR-

70   factors within an hour and a given height interval provides the MTR (*cf.* MTR in Lexicon). The MTR-

71   factor therefore accounts for the distance-dependent variation in monitored volume.

72   Object size [m^2]: Visual profile produced by an object. Reflectivity properties and aspect of the object

73   in respect to the polarisation plane of the beam greatly influence the relationship between the

74   actual object size and the measured RCS.

75   $P_{r_{min}}$ [dBm]: The detection threshold defines the minimal echo size for detection (*cf. STC*).

76   P_t [W]: The transmitted power P_t represents the peak in power transmitted in pulse radar. Pulse

77   radar sequentially emits electromagnetic waves and then listens for the echoes. The electromagnetic

78   waves are created in a magnetron, and transmitted via the antenna.

79   Radar equation: The radar equation defines the main relationship between the echo power received

80   by the radar P_r [W], and properties or the radar (transmitted power P_t [W], antenna gain G_0 [dB],

81   wave length λ [m]), the illuminated object properties (i.e. RCS [m^2]), and it's $distance$ [m] from the

82   radar antenna. The radar equation can be formulated as follows (Drake and Reynolds 2012) eq.

83   3.14a): $P_r = \frac{P_t \cdot G_0^2 \cdot \lambda^2 \cdot RCS}{64 \cdot \pi^3 \cdot distance^4}$.

84   Radiation pattern (antenna diagram): A diagram describing the transmission and receiving
85   characteristics of an antenna for a specific electromagnetic wave length (e.g. X-band). It describes
86   the direction (3D) dependent gain in transmitting and receiving power expressed in decibel (dB), as
87   measured by the manufacturer.

88   RCS [m^2]: The Radar Cross Section describes the reflectivity properties of an object. The RCS is
89   wavelength specific and depends among other things on the reflectivity properties of the object
90   (Eastwood 1967, Drake and Reynolds 2012). Following the radar equation (see Lexicon), the received
91   power P_r is the only object specific quantity measured by non-coherent radar transmitter.
92   Therefore, the RCS can be calculated by correcting the echo size (as a measure of P_r) by the distance
93   (Drake and Reynolds 2012, eq. 4.1): $RCS = \frac{P_r \cdot (4 \cdot \pi)^3 \cdot distance^4}{P_t \cdot G_0{}^2 \cdot \lambda^2}$. We obtain a true RCS only for echoes
94   that transit through the centre of the beam; the RCS is underestimated for all other echoes.

95   STC_{dist} [m]: The Sensitivity Time Control is an adjustable sensitivity setting used to attenuate the
96   received power of signal close to the antenna. The STC sets a time (or distance, since time multiplied
97   by the speed of light gives a distance, e.g. 300 m is about 10^{-6} s) at which the signals are not
98   attenuated any more. In many radar systems available on the market such a STC filter is
99   implemented, as a distance-dependent function, generally unknown to the user. For proper
100   quantifications of small objects, the function should be based on the radar equation (Eastwood
101   1967). STC filters usually act prior to the echo detection and can be further increased post-hoc.

102   Waveguide attenuation [dB]: Attenuation of the transmitted and received power by the waveguide

103   $Width_{beam}$ [m]: The effective beam width for echo detection depends on the object's reflective
104   properties and its distance from the antenna. The variation of the beam width with the distance
105   from the radar defines the monitored volume (Drake and Reynolds 2012). $Width_{beam}$ is calculated
106   for a given object size and distance from the radar antenna, given the following radar parameters
107   (transmitted power P_t, antenna gain G_0, wave length λ, waveguide attenuation, radiation pattern
108   (see R-function "funMTRfactor" in Appendix F).

109

Introduction

110

111   The lowest one to two kilometres of the atmosphere host huge quantities of animal movements,

112   often invisible to the human eye (La Sorte et al. 2015, Hu et al. 2016, Chilson et al. 2017, Bruderer

113   al. 2018). Increasing human aerial activities and the trend towards more and taller constructions

114   increase the collision and mortality risks of these animals aloft (Loss et al. 2015). Thus, there is an

115   increasing demand on monitoring these movements for environmental impact assessments (e.g. at

116   wind farms). Radar systems provide an ideal tool to monitor the temporal and spatial patterns of

117   animal movements locally (Bruderer 1997, Nilsson et al. 2018), as well as on a large scale

118   (Gauthreaux et al. 2003, Chilson et al. 2012, Nilsson et al. this issue). Therefore, the significance and

119   demand for quantitative radar studies on animal movements in the context of ecological or

120   environmental impact assessment studies has increased considerably (Bridge et al. 2011, Bauer and

121   Hoye 2014).

122   An accurate quantification of animal movements requires an adequate, but not easily accessible,

123   knowledge of the monitored volume (Schmaljohann et al. 2008, Drake and Reynolds 2012, Larkin

124   and Diehl 2012). In principal, radars transmit electromagnetic waves that propagate in a three-

125   dimensional beam along a main axis. The shape and extent of the beam defines the volume of air

126   monitored by the radar. The monitored volume can be estimated using the radar equation (see

127   Lexicon, (Eastwood 1967), requiring information on radar parameters and reflectivity properties of

128   the objects. Radar specific parameters (e.g. wave length λ, antenna shape) are readily provided by

129   the manufacturer, but the access to information on adjustable sensitivity settings for echo detection

130   [e.g. detection threshold $P_{r_{min}}$, sensitivity time control (STC_{dist}), see Lexicon] is not guaranteed. In

131   addition to radar properties, the monitored volume strongly depends on the object's size

132   (Schmaljohann et al. 2008). Large objects have a bigger monitored volume than smaller objects

133   (Figure 1a): they are detectable at greater distances along the beam axis, and at wider distances

134   from the beam axis, than smaller objects. However, the actual object size cannot be directly

135   measured by radar. Radar registers the maximal echo intensity (echo size, see Lexicon). Because the

136   echo size decays at a known rate with distance from the radar antenna (power law of four, see radar

137   equation in Lexicon), we can correct the echo size for its distance and obtain a best approximation of

138   the radar cross section (RCS, see Lexicon). The RCS is therefore the echo size corrected for the

139   distance along the main axis, but the RCS is related to the object size only for objects that transit

140   through the beam centre. Because the echo size decreases with increasing distance from the beam

141   axis, objects illuminated in the periphery of the beam will appear smaller (have smaller echo size)

142   than an object of the same size detected in the beam centre (Figure 1b). Therefore, the RCS is a

143   minimal measure of the object size.

144   The frequency at which birds flap their wings is highly correlated with their body size, with larger

145   birds flapping slower than small ones (Pennycuick 2001, Bruderer et al. 2010). This relationship has

146   also been shown in several insect groups (Drake and Reynolds 2012, Greenewalt 1962). The

147   wingbeat frequency of a target can be estimated from the variation in echo intensity over time (echo

148   signature, see lexicon) (Eastwood and Rider 1966, Bruderer et al. 2010, Bruderer and Joss 1969).

149   Therefore, we can use the wingbeat frequency to estimate the size of the target/object,

150   independently from the echo size (Figure 1c). The size distribution of measured targets can then be

151   used to accurately estimate of the size-specific monitored volume for different taxa (Figure 1d).

152   In this study, we analysed six million echoes detected with a vertical-looking radar system (Nilsson et

153   al. 2018), located at a range of sites along the avian African-Eurasian migratory flyway (from Sweden

154   in the north, United Kingdom in the west, to Israel in the south-east), such that birds from a wide

155   geographic range will have been sampled. We used features of the echo signature to classify each

156   echo into four echo-types ("passerine", "wader", "unidentified-bird", and "non-bird"), and estimated

157   the WBF (Zaugg et al. 2008). We first illustrate the influence of adjustable sensitivity settings on the

158   number of detected bird and non-bird echo-types, and its consequences for the monitored volume.

159   We then propose a quantitative framework to estimate the object sizes for echoes with similar

160   wingbeat patterns, and test whether the estimated object sizes are consistent across large

161   geographical ranges that likely differ in the species composition of migratory birds. Finally, we

162   demonstrate the importance of accounting for size-specific monitored volume in order to accurately

163   quantify the height distributions of animal movements aloft. This result highlights the importance of

164   considering the size-specific monitored volume for each echo, and is an important step towards a

165   truly quantitative estimation of animal movements using radar systems.

166
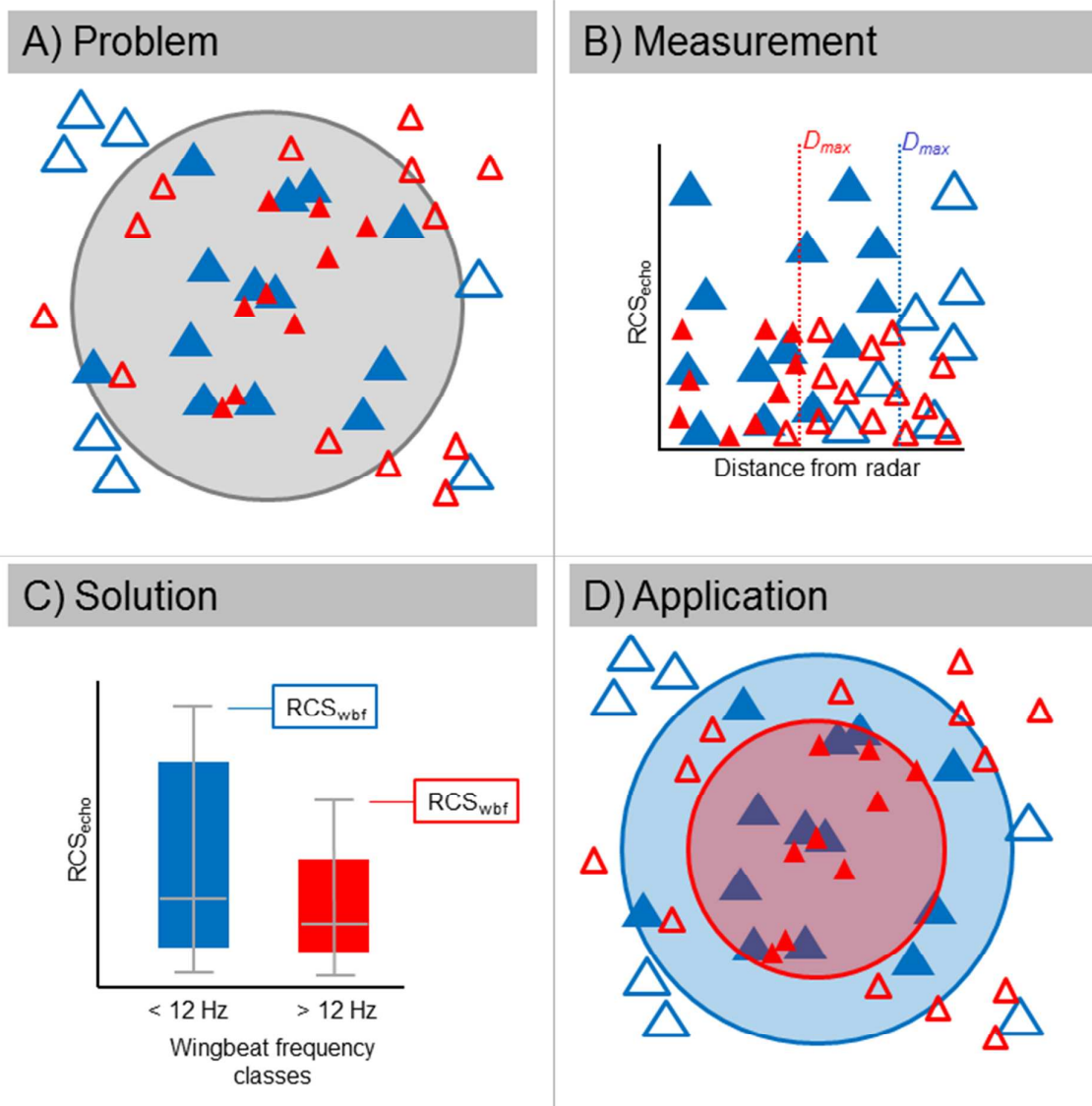
Figure 1: Research scheme. A) Most radar studies assume a maximum detection distance (monitored volume, grey disk) for all detected objects (filled symbols), irrespective of their size (object size: blue > red). However, many small objects remain undetected (open symbols) within the maximum detection distance (red-open symbols within the grey circle). B) Radars detect echoes with large RCS further away than echoes with small RCS (maximal detection distance D_{max} indicated by the vertical dotted line with the respective colour). Because the estimated RCS of objects decreases with increasing distance from the beam axis, the RCS of objects of different size overlap in the low ranges. Therefore, the actual size cannot be directly measured, but C) the wingbeat frequency (WBF) can be used to separate large from small birds (Pennycuick 2001). The upper range of the RCS distributions (RCS$_{wbf}$) should to be closest to the true RCS due to individuals flying across the centre of the beam. D) Applying RCS$_{wbf}$ results in size specific detection monitored volume (blue and red disks).

177

Methods

Echo detection, classification and wingbeat frequency

We used a modified X-band marine radar (Bridgemaster[©], 25 kW, 9.4 GHz, wavelength ca. 3.2 cm) with a vertical-looking 20dB Horn antenna (17.5 ° nominal beam angle at -3 dB; Swiss BirdRadar Solution AG, swiss-birdradar.com). We used 70 ns short-pulse emission for a range resolution of 10 m and a maximal detection range of 1500 m. An automated software detects objects passing through the beam, and digitises the detected echo signals (sampling frequency = 425 – 450 Hz). The digitizer converts the received signal into dBm based on calibration measurements with a signal processing unit and a reference power of 1 mW. The echo signature describes the temporal variation of the echo intensity (see Lexicon). The echo intensity is greatest when objects transit closest to the beam centre. The echo intensity also varies in relation to changes in the aspect of the object, such as the wingbeat movements of birds. To remove the small variations in echo intensity induced by changes in aspect, we apply a low pass filter (Chebyshev type I filters of order 5 with nominal band-pass limit set to 0.5 Hz) on the echo signature to identify the maximal echo intensity (hereafter referred to as echo size [dBm]). Once corrected for the distance according to the radar equation, the echo size is expressed as the radar cross section (RCS [m^2], see Lexicon), assuming objects have the same reflectivity properties. The echo size and its related RCS can strongly depend on the aspect of the animal in relation to the beam orientation (Edwards and Houghton 1959, Bruderer and Joss 1969, Mirkovic et al. 2016). Since vertical-looking radars illuminate animals from below ("ventral aspect"), the influence of aspect variation in a low-pass-filtered RCS is low and thus neglected in this study. For a given object size, the RCS is maximal when the object passes through the beam axis, and minimal at the detection threshold at the periphery of the beam.

We used supervised learning to automate manual echo classification and manual assessment of wingbeat frequency (WBF). A band-pass filter (Chebyshev type I filters of order 5 with nominal band-pass limits set to 4 and 180 Hz) removed high frequency signal oscillations partly due to the 0.8 Hz rotation of the antenna. We used features derived from the echo signature (detailed features in Appendix Table A1) and trained random forest classifiers to group the echoes into four echo-types ("passerine", "wader", "unidentified-bird", and "non-bird"; Zaugg et al. 2008). Class probabilities are calculated for each echo, and the class with the highest probability is assigned to the echo. We re-classified echoes with class probabilities for passerine-type and wader-type lower than 0.5 as unidentified-bird-type. Non-bird echoes are insects and other non-determined objects. We assessed the WBF [Hz] with a random forest regression model trained with manually confirmed WBF values, and features extracted from band-pass echo signatures (detailed features in Appendix Table A1). For

211 each estimated WBF, a credibility factor is provided as the proportion of regression trees reaching

212 close consensus. Cross validation of estimated WBF with manually determined WBF based on expert

213 knowledge shows Pearson correlation coefficient of 0.976 (on a subset of echoes with credibility

214 factors ≥ 0.5). Because of the low-band pass filter (see above), the trained classifier cannot

215 determine WBF below 4 Hz. We restricted the WBF range to 25 Hz for birds (maximal known WBF

216 for European birds, see Bruderer et al. 2010) and to WBF with credibility factors larger than 0.5.

217

218 **Data**

219 We used data from 11 monitoring sites (Table 1): Sempach (Switzerland (CH), year round), Col de

220 Bretolet (CH, autumn), Geneva (CH, spring), Moelle (Sweden (SE), autumn), Sivry (France (FR),

221 autumn), Herzeele (FR, autumn), Upper Galilee (Israel (IL), spring), Arava (IL, spring and autumn),

222 Lower Galilee (IL, spring and autumn), Carmel (IL, spring and autumn), and Falmouth (United

223 Kingdom (UK), year round). During the course of these monitoring campaigns, the deployed radars

224 registered 6,460,205 echoes, of which 660,200 were "passerine-type" echoes (79.5% with WBF),

225 96,337 were "wader-type" echoes (97.8% with WBF), 1,136,481 were "unidentified-bird-type"

226 echoes (44.1% with WBF), and 4,567,187 echoes were classified as "non-bird-type". This latter

227 category undoubtedly consisted largely of insects, which at times can be hugely abundant in the

228 atmosphere (Drake and Reynolds 2012; Hu et al. 2016). We also note that wader-type echoes may

229 also include echoes from bats (Bruderer and Popa-Lisseanu 2005). The WBF of bats range between 5

230 to 12 Hz (similar values to the bird species classified as wader-type), and bats follow similar WBF-

231 body size relationship as birds (Bullen and McKencie 2002, Norberg and Norberg 2012). Further

232 knowledge on cross-validated echo signatures may enable disentanglement of wader-type bird-

233 echoes from bat-echoes. The monitoring campaigns differed in sensitivity settings: STC_{dist} ranged

234 from 100 m to 500 m, and detection threshold $P_{r_{min}}$ ranged from -100 dBm to -90 dBm.

235

236 Table 1: Overview of the 11 sites with radar monitoring: the geographic location (CH: Switzerland, SE: Sweden,

237 FR: France, IL: Israel) and the monitoring period are provided, however the operation of the radar during these

238 periods was not always continuous.

Site	Latitude, Longitude	Altitude [m asl]	Start	End	Monitoring days (hours)
Sempach (CH)	47.1, 8.2	450	Mar. 2016	Jun. 2017	504 (9707)
Geneva (CH)	46.2, 6.0	395	Mar. 2017	Jun. 2017	72 (1569)

Col de Bretolet (CH)	46.2, 6.8	1200	Aug. 2016	Oct. 2016	72 (1325)
Moelle (SE)	56.3, 12.5	70	Sep. 2015	Nov. 2015	62 (1384)
Herzeele (FR)	50.9, 2.5	10	Aug. 2016	Oct. 2016	59 (1124)
Sivry (FR)	48.8, 6.2	250	Oct. 2016	Nov. 2016	47 (967)
Upper Galilee (IL)	32.9, 35.2	350	Sep. 2015	Nov. 2015	66 (1417)
			Feb. 2016	May 2016	95 (2132)
Arava (IL)	30.7, 35.0	15	Mar. 2016	May 2016	81 (1911)
			Aug. 2016	Nov. 2016	79 (1795)
Lower Galilee (IL)	32.6, 35.4	115	Mar. 2016	Jun. 2016	77 (1799)
			Aug. 2016	Nov. 2016	92 (2168)
Carmel (IL)	32.6, 35.1	250	Aug. 2016	Nov. 2016	94 (2144)
Falmouth (UK)	50.2, -5.1	120	Mar. 2015	Mar. 2017	483 (5993)

239

Analyses

Influence of sensitivity settings and object size on monitoring volume

Using calculations based on the radar equation (see Lexicon), we illustrate the influence of adjustable sensitivity settings (detection thresholds $P_{r_{min}}$: -93 dBm, -87 dBm) and object diameter (5 cm or 15 cm) on the monitored volume, especially on the maximum detection distance (D_{max}), and on MTR-factors. The MTR-factor is the ratio between a 1-km transect line and the effective beam width at the distance of detection (see Lexicon). The MTR-factors thus account for size-specific and distance dependent variation in effective beam width, and represent contribution of each echo to MTR. We compute the effective beam width for each 1 m using an R-function based on the radar equation (Appendix F, R-function "funMTRfactor") and the following parameter: STC_{dist} 300 m, P_t 20 kW, and waveguide attenuation 0 dB. We further report the median of MTR-factors per 50 m distance bin.

Influence of sensitivity settings on number of detected echoes

We investigated the influence of adjustable sensitivity settings on the number of detected echoes for each echo-type. We applied the following post-hoc (i.e. after echo detection) sensitivity settings: $P_{r_{min}}$ of -90 dBm, -87 dBm, -83 dBm, and STC_{dist} of 500 m. We used all data monitored with a maximal $P_{r_{min}}$ -93 dBm and STC_{dist} 300 m and we report changes in number of echoes detected for each echo-type: passerine, and non-bird.

11

259 An increase of three dB of the detection threshold $P_{r_{min}}$ (a logarithmic scale) corresponds to a two

260 fold increase in the required echoed energy for detection. With an increase of the detection

261 threshold $P_{r_{min}}$, only echoes with an echo size larger than the post-hoc detection threshold remain

262 in the dataset. Within the STC range, when the $distance$ [m] of the object from the radar antenna is

263 smaller than STC_{dist} [m], the effective threshold $P_{r_{min|stc}}$ [dBm] is higher than the detection

264 threshold settings $P_{r_{min}}$ [dBm]:

265 $$P_{r_{min|stc}} = \begin{cases} P_{r_{min}} - 40\,log_{10}(distance/STC_{dist}), & distance < STC_{dist} \\ P_{r_{min}}, & distance \geq STC_{dist} \end{cases} \text{(Eq. 1)}$$

266 While $distance < STC_{dist}$, the STC-function effectively sets a minimal RCS for detection RCS_{min}.

267 Indeed, reformulating the STC-function in W (*cf.* dB in Lexicon) gives $P_{r_{min|stc,W}} = P_{r_{min,W}} \cdot \frac{STC_{dist}^4}{distance^4}$

268 (Eq. 2); Eq. 2 inserted into the radar equation (*cf.* RCS in Lexicon) further gives: $RCS_{min} =$

269 $\frac{P_{r_{min|stc,W}} \cdot (4 \cdot \pi)^3 \cdot distance^4}{P_{t,W} \cdot G_0^2 \cdot \lambda^2} = \frac{P_{r_{min,W}} \cdot (4 \cdot \pi)^3 \cdot STC_{dist}^4}{P_{t,W} \cdot G_0^2 \cdot \lambda^2}$ (Eq. 3). Therefore, RCS_{min} is independent on the

270 detection distance. With an increase of the STC, only echoes with a RCS larger than or equal

271 to RCS_{min} remain in the dataset.

272

Determination of object size using wingbeat frequency

274 We estimate the object size of birds for each echo type and WBF intervals of 2 Hz. We report the

275 0.9- and 0.95-quantiles of the RCS distribution for each echo-type and 2 Hz WBF intervals

276 [$object\ diameter = 2 \cdot (RCS/\pi)^{1/2}$, assuming an ideal spherical shape]. The species composition

277 likely differs between the different geographical areas, and during spring and autumn migration

278 events. We investigated whether the geographical region influences the observed RCS distributions.

279 We used passerine-type echoes only because they are classified with high credibility, abundant on

280 each site and cover the entire range of WBF. We tested the dependency of the 0.9-quantile of the

281 RCS (transformed as *object diameter*, see above; using the 0.95-quantiles lead to quantitatively

282 similar results) on WBF 2-Hz interval (as ordered factors), adding the site identity as a random

283 intercept in linear mixed-effects models as implemented in the "lme4" R-package (Bates et al. 2015,

284 R-version 3.4.3), assuming a Gaussian distribution of the residuals.

285

Distance distribution corrected for size specific monitored volume

287   To demonstrate the influence of MTR-factors on the estimate of migration intensity, we compared

288   the distance distribution of the detected echoes with the distance distribution of MTR-factors. For

289   each type of bird echo and WBF, we used the 0.90-quantile distribution of RCS (analyses with the

290   0.95 quantile were quantitative similar). The calculation of MTR-factor for each echo requires the

291   following information: the estimated object size (0.90-quantile distribution of RCS per echo type and

292   2 Hz WBF interval, see Appendix Table A2), the distance (echoes are binned into 50 m distance

293   intervals), the effective detection thresholds $P_{r_{min}}$ (see Eq. 1), the transmitted power P_t specified by

294   the radar type, and the radiation pattern (see Lexicon) as provided by the antenna manufacturer

295   (Appendix F, R-function "funMTRfactor"). We calculated the MTR-factors for all bird echoes

296   registered with maximum $P_{r_{min}}$ of -93 dBm and STC_{dist} of 300 m, so that echo detection is based on

297   a radar beam of the same shape.

298

299

Results

301   *Influence of sensitivity settings and object size on monitoring volume*

302   An increase of the detection threshold by 6 dB reduced the effective beam area (planar projection of

303   the monitored volume along the distance axis) by about 50% (Figure 2: $P_{r_{min}}$ -93 dBm *vs.* -87 dBm,

304   see also Table A3 in Appendix). In particular, the maximal detection distance D_{max} decreased from

305   1361 m ($P_{r_{min}}$ -93 dBm) to 949 m ($P_{r_{min}}$ -87 dBm) for objects of 15 cm, and from 765 m ($P_{r_{min}}$ -93

306   dBm) to 527 m ($P_{r_{min}}$ -87 dBm) for objects of 5 cm (Table A3, Figure 2). In contrast, an increase of

307   STC_{dist} from 300 m to 500 m only had a minor effect on the beam area (<10 %, Table 3) and does

308   not affect the maximum detection distance as long as the object is large enough to be detected

309   within the STC range.

310   The MTR-factors are inversely proportional to the effective beam width (see Lexicon). Setting higher

311   detection threshold $P_{r_{min}}$ reduces the maximal detection distance D_{max}, and the MTR-factors above

312   D_{max} are undefined and set equal to zero. Within D_{max}, setting higher detection threshold or STC

313   reduces the effective beam width, therefore increases the MTR-factors at a given height. Similarly, at

314   a given height, the MTR- factors of large objects are smaller than the MTR-factors of small objects.
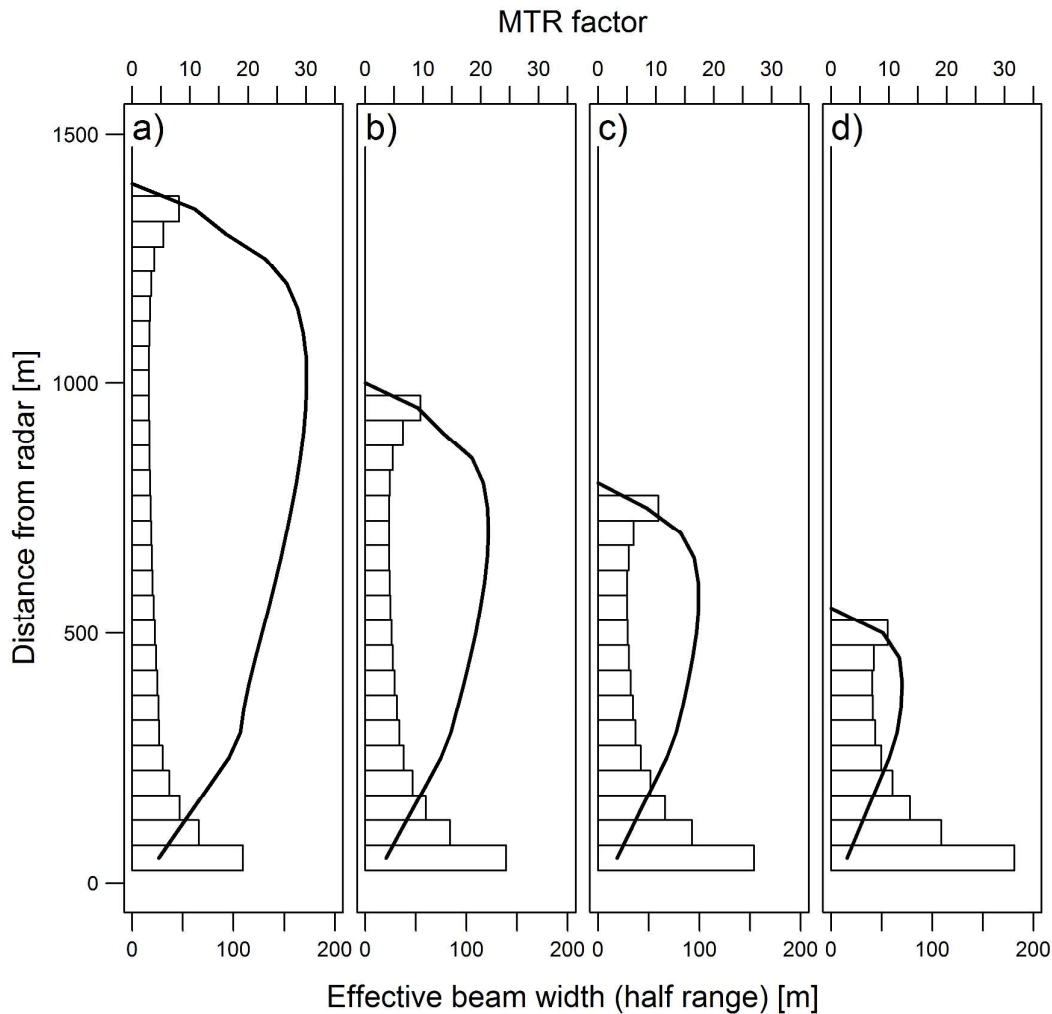
Figure 2: Effective beam width (half-range, solid lines, bottom x-axis) and MTR-factors (bars, 50 m distance bin, top x-axis) in relation to the distance for a) -93 dB $P_{r_{min}}$ and 15 cm object diameter (RCS = 0.0177 m^2), b) -87 dB $P_{r_{min}}$ and 15 cm object diameter, c) -93 dB $P_{r_{min}}$ and 5 cm object diameter (RCS = 0.0020 m^2), d) -87 dB $P_{r_{min}}$ and 5 cm object diameter. Further parameters to calculate the effective beam width: STC_{dist} 300 m, P_t 20 kW, and waveguide attenuation 0 dB (see R-function in Appendix).

Influence of sensitivity settings on number of detected echoes

An increase of the detection threshold and STC lowers the measurement sensitivity and reduces the number of detected echoes (Table 2, Figure 3). Obviously, a reduction of the sensitivity increases the minimal RCS for detection RCS_{min} (Table 2). In terms of echo detection, the effects of an increase of the detection threshold or of the STC differ (Figure 3). By increasing the STC, small objects, especially echoes classified as non-bird type, are reduced considerably. The proportion of non-bird echoes

328   decreases from 59% (Table 2: STC_{dist} 300 m, $P_{r_{min}}$ -93 dBm) to less than 20% of the detected

329   echoes (Table 2: STC_{dist} 500 m, $P_{r_{min}}$ -93 dBm). This 200 m increase of STC excluded 89% of the

330   non-bird echoes, but only 28% of the passerines-type echoes. Increasing the detection threshold not

331   only excludes small objects, it also reduces the monitored volume for any given object size. An

332   increase in the detection threshold (-93 dBm to -90 dBm; Table 2) decreases the proportion of non-

333   bird echoes to 42 % by excluding 67% of theses echoes, but this also leads to an exclusion of 30% of

334   the passerine-type echoes.

335

336   Table 2: Influence of sensitivity settings (STC_{dist} and $P_{r_{min}}$) on the minimal RCS for detection RCS_{min}, the

337   number of echoes, and the proportion of passerine-type and non-bird-type echoes. The total number of

338   echoes also include wader-type and unidentified-bird-type echoes.

STC_{dist}[m]	$P_{r_{min}}$ [dBm]	RCS_{min} [cm²]*	N. echoes	Proportion of echoes	
				Passerine	Non-bird (Insect)
300	-93	0.36	2915284	0.181	0.589
300	-90	0.72	1330121	0.279	0.423
300	-87	1.43	664900	0.381	0.224
300	-83	3.60	282270	0.418	0.064
500	-93	2.77	1108448	0.342	0.171
500	-90	5.54	455769	0.369	0.047
500	-87	11.04	193102	0.265	0.020
500	-83	27.74	52868	0.085	0.015

339   *using antenna gain G_0= 20 dB; transmitted power $P_{t,W}$ = 20 kW; see Eq. 3.

340
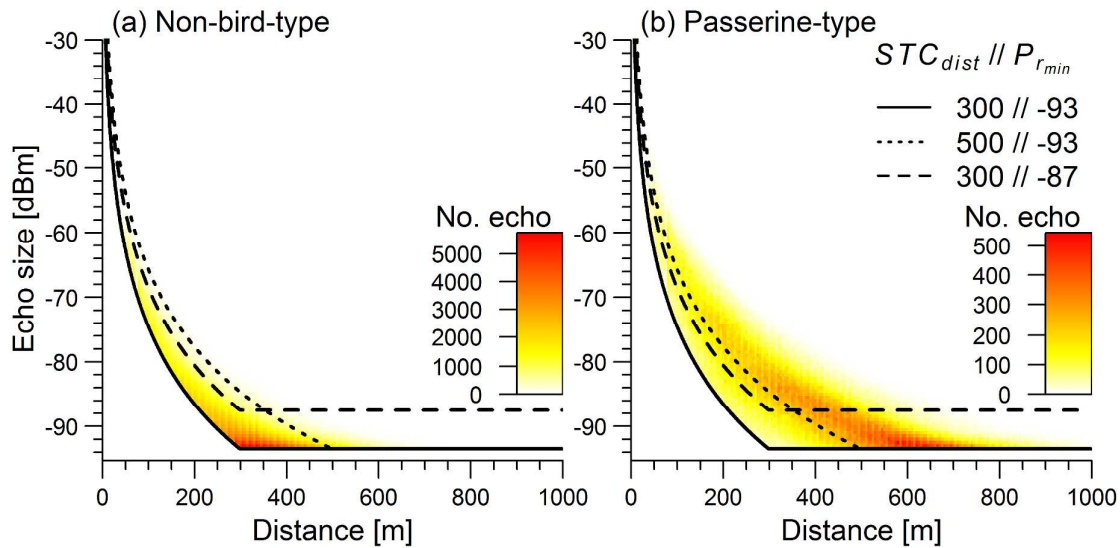
Figure 3: Echo size in relation to detection distance for a) non-bird-type echoes (mostly "insect") and b) passerine-type echoes. Lines delimit distance dependent detection thresholds $P_{r_{\min|stc}}$ (Eq. 1): i) STC_{dist} 300 m and $P_{r_{min}}$ -93 dBm (solid line), ii) STC_{dist} 500 m and $P_{r_{min}}$ -93 dBm (dotted line), and iii) STC_{dist} 300 m and $P_{r_{min}}$ -87 dBm (dashed line). Note the different scale of the number of echo between non-bird-type and passerine-type echoes.

Determination of object size using wingbeat frequency

The RCS decreased with increasing WBF for all three types of bird echoes (Figure 4). Considering echoes with similar WBF, the median RCS is smallest for passerine-type, generally highest for wader-type, whereas unidentified birds tend to show intermediate median values. The 0.9-quantile distributions of RCS parallel the 0.95-quantile distributions.

Wader-type echoes with low WBF (4 – 10 Hz) typically fell within the 12 – 13 cm diameter range. The wader-type echoes with 11 ± 1 Hz WBF had smaller 0.95 (or 0.90) RCS quantiles than echoes with 13 ± 1 Hz WBF. The relatively few wader-type echoes with WBF larger than 13 Hz only occurred in non-rotation mode and mostly occurred during night time. Passerine-type echoes with low WBF (4 – 12 Hz) had 0.95 RCS quantiles of 7 – 8 cm diameters. We observed a marked decrease in RCS between 11 Hz and 13 Hz WBF intervals. The RCS of passerines with WBF > 12Hz decreased steadily to a minimal 0.95-quantile diameter of 3.1 cm. Unidentified-bird-type echoes showed a steeper decrease in 0.95-quantiles between 5 Hz and 13 Hz WBF intervals than between 13 Hz and 25 Hz WBF intervals.

362   The 0.95-quantiles of RCS per 2 Hz WBF intervals for passerine-type echoes showed no differences

363   between study site (using the 0.90 RCS quantiles were quantitatively similar). Between-site variance

364   (0.22 ± 0.73) is about 20 times smaller than the averaged site value (Intercept 4.55 ± 0.08) and 10

365   times smaller than the decrease in RCS per two-Hertz (-2.34 ± 0.18; see also Figure S3 in Appendix E).

366

a) Passerine-type   **b) Unidentified-bird-type**   **c) Wader-type**
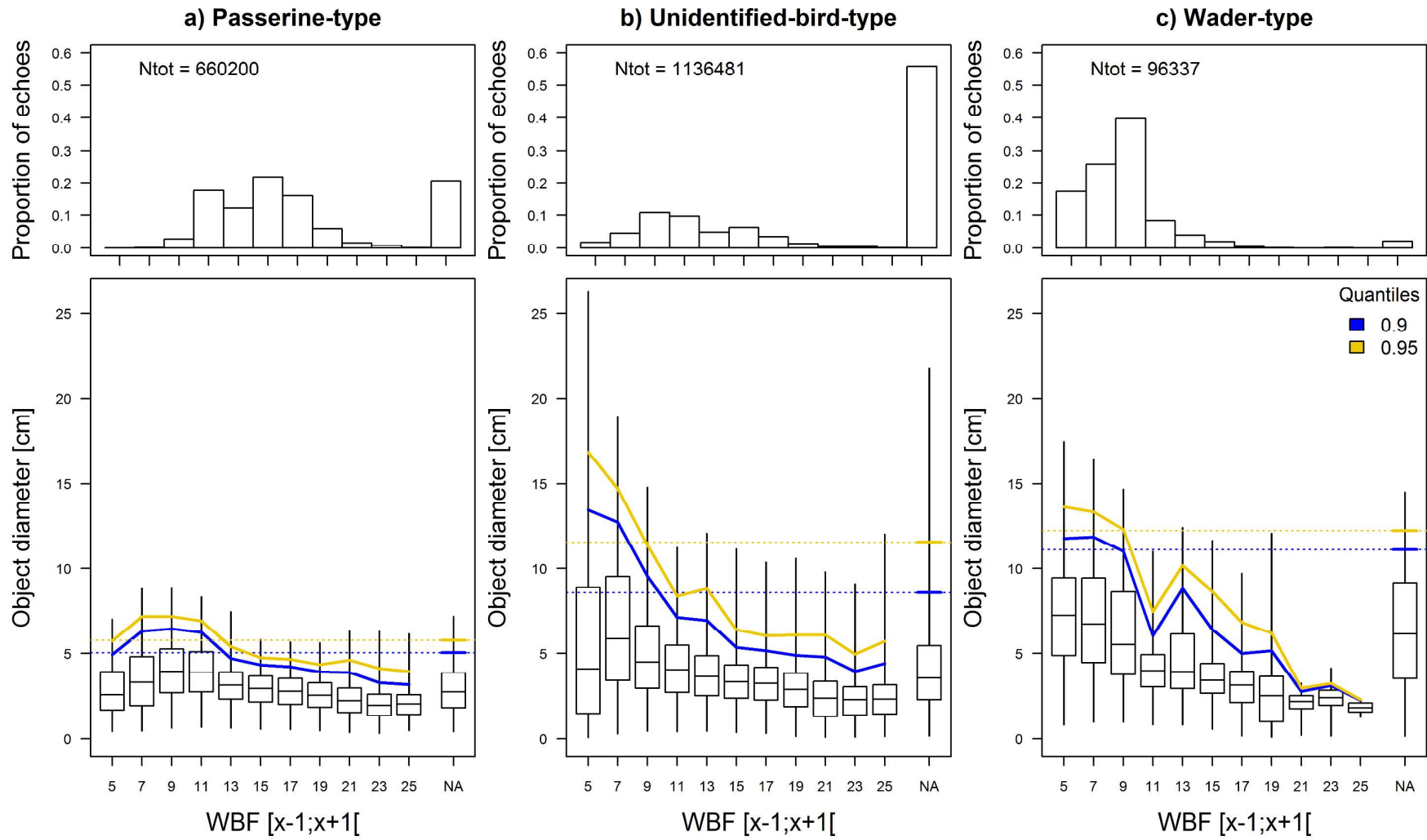
367
368   *[legend see next page]*

369   Figure 4: Distributions of registered object diameters (cm, $object\ diameter = 2 \cdot (RCS/\pi)^{1/2}$, assuming an

370   ideal spherical shape) per 2 Hz WBF intervals for echoes of a) passerine-type, b) unidentified-bird-type, and c)

371   wader type. Boxes show the 0.25 and 0.75 quantiles (vertical lines are the 0.01 and 0.99 quantiles). Coloured

372   lines indicate the 0.9 (blue) and 0.95 (yellow) quantile of the distributions of object diameters per WBF-

373   interval. Sample size (proportion of echo) indicated on top panels.

374

375   *Distance distribution corrected for object-size dependent beam width*

376   After correction for the monitored volume with MTR-factors, the height distribution of the MTR is

377   lower than the height distribution of detected echoes (Figure 5). Fifty percent of the echoes were

378   detected above the first 428 m (0.25-quantile: 266 m; 0.75-quantile: 597 m, Figure 5a), whereas 50%

379   of the MTR occurred within the first 306 m (0.25-quantile: 167 m; 0.75-quantile: 499 m, Figure 5b).

380   The lower distribution of MTR compared to the distribution of echo detection is due to the

381   correction applied for a narrower beam width at short distance compared to mid-distances (Figure

382   2). The distance distributions of MTR depend on the maximal detection distance D_{max} of the

383   different taxa, as calculated with the 0.90 RCS quantiles (see Appendix Table A2), although some

384   echoes are detected further. According to the assumed object size per taxa, D_{max} of large

385   passerines (passerine-type with WBF < 12 Hz) is 858 m, and D_{max} of small passerines echoes

386   (passerine-type with WBF >12Hz) is 723 m (Figure 5). Beyond 723 m, the MTR-factors of passerine-

387   type echoes with WBF > 12 HZ equals zero, and therefore beyond this limit movements of small-

388   passerine are ignored.

389
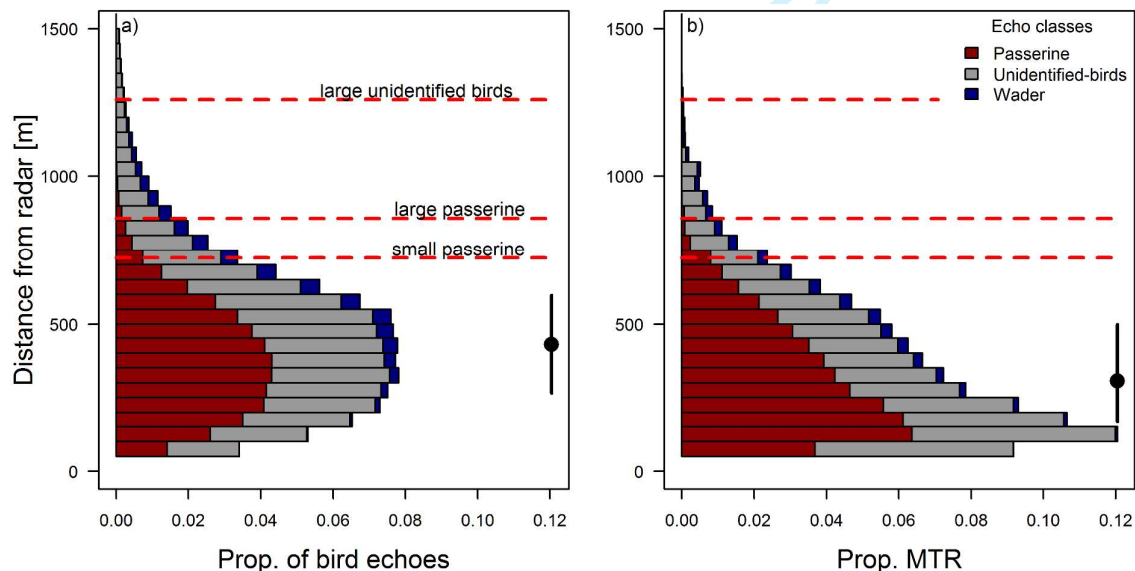
390

391 Figure 5: Distance distributions of a) echoes and b) MTR (MTR- factors according to the 0.90 RCS quantile for

392 each echo type and WBF interval). Colours indicate echoes of different echo-types: red for passerine-type, grey

393 for unidentified-bird-type, and blue for wader-type. The vertical black lines indicate the 0.25- and 0.75-

394 quantiles, the dots indicate the 0.50-quantiles of the distance distributions. The horizontal red dashed lines

395 indicate the maximal detection distances D_{max} ($P_{r_{min}}$ = -93 dBm, $P_{t,W}$= 20 kW, waveguide attenuation = 0

396 dB) for small passerine type (object diameter = 4.7 cm), large passerine type (object diameter = 6.5 cm), and

397 large unidentified birds (object diameter = 13.5 cm). Above these lines, the MTR-factors equal zero for the

398 respective echo groups.

399

400 Discussion

401 The typical assumption made by many radar operators, that all birds are detected within the

402 maximal distance of bird detection, will lead to erroneous conclusions. This study provides a

403 framework for the accurate quantification of avian movements with radar, taking account of the

404 size-specific monitored volume. Using data collected from widely-separated areas across Europe,

405 and a large range of flying animals, we estimated the size of a bird based on the WBF, independent

406 of the echo size.

407

408 *Influence of sensitivity settings*

409 In this study, we demonstrate the effects of adjustable sensitivity settings on the detection of echoes

410 of diverse types. Increasing the STC effectively removes small non-bird echoes. This is especially

411 important because of the huge number of non-bird echoes (2/3 of all detected echoes), and a small

412 probability of miss-classification can produce an elevated number of bird-type resulting from

413 detection and misclassification of echoes from non-bird objects (insects). The STC also has the

414 advantage of acting only within the distance set by the STC, so it does not reduce the maximal

415 detection distance of the target objects. In contrast, increasing the detection threshold significantly

416 reduces the surveyed volume. For instance, increasing the detection threshold substantially

417 decreases the maximal detection distance of small birds. Beyond this distance, the radar only

418 monitors movements of larger birds.

419 When possible, sensitivity settings should be selected to maximise echo detection. For a quantitative

420 monitoring of avian migration, sensitivity settings (i.e. STC and detection threshold) should be

421 appropriately selected in order to monitor movements of small birds. Setting high STC values post-

422 hoc can remove echoes from small birds in studies that focus on large birds only (e.g. geese).

423   Therefore, adjusting the STC is an effective tool to match the specific aim and target object of radar

424   monitoring, and using the appropriate radar parameters then correct for differences in the surveyed

425   volume.

426   Knowledge of radar parameters (wave length, peak of transmitted power, antenna gain, waveguide

427   attenuation, and the radiation pattern) and adjustable sensitivity settings (detection threshold and

428   STC) are a prerequisite for any quantitative radar monitoring. Moreover, regular calibration will

429   ensure registering of accurate information on standardised echo properties such as the echo size

430   and its derived RCS (Atlas 2002, Schmaljohann et al. 2008, Urmy and Warren 2017, May et al. 2017,

431   Drake and Reynolds 2012). Unfortunately, popular radar systems operating with built-in analysis

432   software may not provide information on radar parameters and adjustable sensitivity settings to the

433   end-users. In addition, some end-users can only monitor the radar display, not being able to register

434   any quantitative information on the echo size (Nilsson et al. 2018). Such black-box radar systems

435   render difficult any quantitative assessment of animal movements. As demonstrated in this study,

436   the striking effects of adjustable sensitivity settings on the number of detected echoes per echo-type

437   render the calibration and report of these sensitivity settings essential for any quantitative radar

438   measurement.

439

440   *Determination of object size using WBF*

441   We estimated the object size from the echoed RCS for each echo-type (passerine-type, wader-type,

442   and unidentified-bird-type) and WBF (2 Hz intervals). The smaller RCS of echoes with high WBF

443   compared to echoes with lower WBF corroborate the negative correlation between body size and

444   WBF defined in allometric flight models (Bruderer et al. 2010, Pennycuick 2001). The fact that the

445   estimated RCS are independent from the study site and season provides support to the general

446   validity of using WBF to estimate the object size.

447   Using the 0.90- or 0.95-quantile of the RCS distributions provides bird size estimates close to

448   experimental measurements on birds measured on the broad side (Edwards and Houghton 1959,

449   Bruderer and Joss 1969, Vaughn 1985). Deviation from the relationship between the WBF and the

450   related bird size can occur because of variation in flight behaviour. For instance, many passerine-

451   type echoes with WBF lower than 8 Hz may originate from swallows performing flap-gliding flight

452   instead of flap-bounding flight (Rayner 1985, Liechti and Bruderer 2002, Tobalske 2007). Passerines

453   contribute to the large majority of inland avian migrations fluxes (Hahn et al. 2009), and probably

454   the majority of the unidentified-bird-type echoes are from passerine birds. Changes in the

455   orientation of the bird's body within the beam can induce important changes in echo intensity,

456   masking the regular modulation of the echo intensity due to the wingbeat patterns. Unidentified-

457   bird-type echoes do not show a clear wingbeat type and less than 50% of the echoes had a credible

458   WBF. Nevertheless, compared to passerine-type echoes, the upper RCS distribution of unidentified-

459   bird-types is larger, probably because unidentified-bird-type echoes also include echoes from large

460   soaring birds and bird flocks, shifting the RCS distributions to larger quantiles. Consequently, the

461   over-estimation of the 0.90 RCS quantiles for unidentified-bird-type echoes leads to smaller MTR-

462   factors, and an underestimation of the standardised movement intensity (MTR). The maximal WBF

463   of wader-type birds reaches 12 Hz, with the notable exception of quails *Coturnix coturnix* (16Hz,

464   Bruderer et al. 2010) and other echoes with WBF > 12 Hz are probable miss classifications.

465   The RCS used in this study is not corrected for the decay in echo intensity with increasing distance

466   from the beam axis. The rotation of the antenna on a slight nutated axis can allow the estimation of

467   the angle between the entry- and exit-point of the object in the beam in relation to the beam centre.

468   Assuming a straight flight, this angle can be used to calculate the closest distance between the

469   object and the centre of the beam, and thus to correct the RCS accordingly (Drake and Reynolds

470   2012). This requires an accurate estimation of the beam width, and has not yet been implemented in

471   the radar system used in this study. We here proposed a method to determine the RCS according to

472   the WBF, independently of the position of the object within the beam.

473   A similar approach could estimate the monitored volume for insects. Insects also show strong

474   relationships between WBF and body size (Drake and Reynolds 2012, Greenewalt 1962). However,

475   this relationship only holds within particular taxonomic groups, as insect taxa differ very much in size

476   and wing shape. The estimation of insects' RCS based on WBF thus requires more detailed echo

477   classification, or knowledge on flight phenology.

478

479   *Distance distribution corrected for object-size dependent beam width*

480   After correction for the monitored volume, the height (i.e. distance for a vertical looking antenna)

481   distribution of the migration intensity is lower than if only reporting the height distribution of

482   detected echoes. For instance, 50 % of the detected echoes were above 428 m agl, and after

483   correction for the variation in monitored volume, 75 % of the animal movement intensity occurred

484   below 499 m agl and even 50 % of the animal movement intensity occurred below 306 m agl. The

485   differences in the height distribution of echoes and MTR highlight the potential misleading

486   evaluation of collision risks of animals with human made structures such as wind turbines, bridges or

487   power lines. In that regard, it is crucial that impact assessment studies accurately quantify the
488   intensity of animal movements.

489   This article demonstrates the importance of reporting standardised movements such as MTR to
490   avoid detection biases. Equally important is to report the maximal detection ranges (see Figure 5)
491   because important migration intensity can occur at high altitude (reviewed in Bruderer and Peter
492   2017, Bruderer et al. 2018), far above the maximal detection range of a particular monitoring
493   scheme. Quantitative information on high migration events can be retrieved using longer pulse
494   emission that increase the maximal detection distance (with the use of lower detection threshold
495    $P_{r_{min}}$). Alternatively, the increasing availability of weather radar data can complement height
496   distribution retrieved from small scale radar systems (Nilsson et al. 2018).

497

498   *Conclusions*

499   Radar systems are valuable tools for the monitoring of aerial animal movements, but the results may
500   suffer from important biases when the registered data is not processed adequately. In line with
501   recent publications which detail adequate procedures (Schmaljohann et al. 2008, Drake and
502   Reynolds 2012, Urmy and Warren 2017, May et al. 2017, Larkin and Diehl 2012) we hope that this
503   publication will help to improve the scientific quality of radar monitoring.

504   We demonstrate the importance of accurately quantifying animal movement intensities, in
505   particular for impact assessment studies of human-made structures (Aschwanden et al. 2018), or
506   more generally to ecological studies of bioflows (Hu et al. 2016). Fixed-beam radar systems have the
507   great advantage of being able to retrieve detailed information on the registered echoes, such as the
508   WBF. We show how the WBF can be used as an independent measure of the body size of the animal,
509   and how this taxa-specific RCS provides the most accurate estimation of the surveyed volume. When
510   information on WBF is missing, expert knowledge on the body size (and its estimated RCS) can allow
511   the estimation of the surveyed volume. Together with specific information on radar parameters
512   (transmitted power, antenna gain, wave length, radiation pattern) and sensitivity parameters
513   (detection threshold, STC), information on the taxa specific RCS are essential for any quantitative
514   monitoring of animal movement and should always be made available and reported.

515

516

Contributions

517

518 BS and FL conceived the study. BS, MB, SCV, JWC collected the data. BS, FL, SZ conducted the

519 analyses. BS wrote the manuscript with substantial contributions from all authors.

520

Data availability

522 Data used for this study are deposited on Zenodo: [doi upon acceptance]

523

Acknowledgements

531

532

References

534 Aschwanden, J. et al. 2018. Bird collisions at wind turbines in a mountainous area related to bird
535   movement intensities measured by radar. – Biol. Conserv. 220: 228–236.

536 Atlas, D. 2002. Radar calibration: some simple approaches. – Bull. Amer. Meteor. Soc. 83: 1313–
537   1316.

538 Bates, D. et al. 2015. lme4: Linear mixed-effects models using Eigen and S4. R package version 1.1--7.

539 Bauer, S. and Hoye, B. J. 2014. Migratory animals couple biodiversity and ecosystem functioning
540   worldwide. – Science 344: 1242552.

541 Bridge, E. S. et al. 2011. Technology on the move: recent and forthcoming innovations for tracking
542   migratory birds. – BioScience 61: 689–698.

543 Bruderer, B. 1997. The study of bird migration by radar. Part 2: Major achievements. –
544   Naturwissenschaften 84: 45–54.

545 Bruderer, B. et al. 2010. Wing-beat characteristics of birds recorded with tracking radar and cine
546   camera. – Ibis 152: 272–291.

547 Bruderer, B. et al. 2018. Vertical distribution of bird migration between the Baltic Sea and the
548   Sahara. – J. Ornithol. 41: 282.

549 Bruderer, B. and Joss, J. 1969. Methoden und Probleme der Bestimmung von Radarquerschnitten
550   freifliegender Vögel. – Rev. suisse Zool. 76: 1106–1118.

551 Bruderer, B. and Peter, D. 2017. Windprofit favouring extreme altitudes of bird migration. – Ornithol.
552   Beob. 114: 73–86.

553 Bruderer, B. and Popa-Lisseanu, A. G. 2005. Radar data on wing-beat frequencies and flight speeds
554   of two bat species. – Acta Chiropterol. 7: 73–82.

555 Bullen, R. D. and McKencie, N. L. 2002. Scaling bat wingbeat frequency and amplitude. – J. Exp. Biol.
556   205: 2615–2626.

557 Chilson, P. B. et al. 2012. Radar aeroecology: exploring the movements of aerial fauna through radio-
558   wave remote sensing. – Biol. Lett. 8: 698–701.

559 Chilson, P. B. et al. (eds.) 2017. Aeroecology - Springer International Publishing.

560 Drake, V. A. and Reynolds, D. R. 2012. Radar entomology. Observing insect flight and migration -
561   CABI.

562 Eastwood, E. 1967. Radar Ornithology - Methuen.

563 Edwards, J. and Houghton, E. W. 1959. Radar echoing area polar diagrams of birds. – Nature 184:
564   1059.

565 Gauthreaux, S. A. et al. 2003. Using a network of WSR-88D weather surveillance radars to define
566   patterns of bird migration at large spatial scales. – In: Berthold, P. et al. (eds.), Avian migration.
567   Springer, pp. 335–346.

568 Greenewalt, C. H. 1962. Dimensional relationships for flying animals. – Smithsonian Miscellaneous
569   Collections 144.

570 Hahn, S. et al. 2009. The natural link between Europe and Africa - 2.1 billion birds on migration. –
571   Oikos 118: 624–626.

572 Hu, G. et al. 2016. Mass seasonal bioflows of high-flying insect migrants. – Science 354: 1584–1587.

573 La Sorte, F. A. et al. 2015. Seasonal changes in the altitudinal distribution of nocturnally migrating
574   birds during autumn migration. – R. Soc. Open Sci. 2: 150347.

575 Larkin, R. P. and Diehl, R. H. 2012. Radar techniques for wildlife research. – In: Silvy Nova J. (ed.),
576   Techniques for wildlife manual. The John Hopkins University Press, pp. 319–335.

577 Liechti, F. and Bruderer, L. 2002. Wingbeat frequency of barn swallows and house martins: a
578   comparison between free flight and wind tunnel experiments. – J. Exp. Biol. 205: 2461–2467.

579   Loss, S. R. et al. 2015. Direct mortality of birds from anthropogenic causes. – Annu. Rev. Ecol. Evol.
580   Syst. 46: 99–120.
581   May, R. et al. 2017. Performance test and verification of an off-the-shelf automated avian radar
582   tracking system. – Ecol. Evol. 7: 5930–5938.
583   Mirkovic, D. et al. 2016. Electromagnetic model reliably predicts radar scattering characteristics of
584   airborne organisms. – Sci. Rep. 6: 35637.
585   Nilsson, C. et al. 2018. Field validation of radar systems for monitoring bird migration. – J. Appl. Ecol.
586   278: 3074.
587   Norberg, U. M. L. and Norberg, R. Å. 2012. Scaling of wingbeat frequency with body mass in bats and
588   limits to maximum bat size. – J. Exp. Biol. 215: 711.
589   Pennycuick, C. J. 2001. Speeds and wingbeat frequencies of migrating birds compared with
590   calculated benchmarks. – J. Exp. Biol. 204: 3283–3294.
591   Rayner, J. M. V. 1985. Bounding and undulating flight in birds. – J. Theor. Biol. 117: 47–77.
592   Schmaljohann, H. et al. 2008. Quantification of bird migration by radar - a detection probability
593   problem. – Ibis 150: 342–355.
594   Tobalske, B. W. 2007. Biomechanics of bird flight. – J. Exp. Biol. 210: 3135–3146.
595   Urmy, S. S. and Warren, J. D. 2017. Quantitative ornithology with a commercial marine radar:
596   Standard-target calibration, target detection and tracking, and measurement of echoes from
597   individuals and flocks. – Methods Ecol. Evol. 8: 860–869.
598   Vaughn, C. R. 1985. Birds and insects as radar targets: a review. – Proceedings of the IEEE 73: 205–
599   227.
600   Zaugg, S. et al. 2008. Automatic identification of bird targets with radar via patterns produced by
601   wing flapping. – J. R. Soc. Interface 5: 1041–1053.
602
603

604   Supplementary information

605   Appendix A) **Features used for the echo classification and WBD estimation**

606   **Table A1**: *Description of features used for the echo classification and WBF assessment.*

Feature category	Description	Used for
Fundamental Frequency Estimators (FFE)	These features are 'weak' estimators of the fundamental frequency of a signal. If WF pattern is absent, the feature still has a numeric value. If WF pattern is present, generally only a subset of the values are valid approximations.	Echo classifier and WFF estimator
FFE-prominence	These features estimate the prominence of the spectral peaks used for the FFE and can be understood as a rough metric of quality for these features	Echo classifier and WFF estimator
Radar Cross Section (RCS)	This is an estimator of Radar Cross Section i.e. a target's intrinsic reflectivity which is a crude approximation of a target's size. It often underestimates the actual size.	Echo classifier only
Relative Magnitude of Fluctuations	These features estimate the relative magnitude of fluctuations in target's reflectivity.	Echo classifier only

607

608

609   Appendix B) **Estimated object size**

610   ***Table A2****: Table of estimated object size from the 0.90 RCS quantile, assuming a spherical shape of*

611   *the birds:* $object\ diameter = 2 \cdot (RCS_{0.90}/\pi)^{1/2}.$

WBF [Hz]	Object diameter [cm]		
	Unidentified-bird-type	Passerine-type	Wader-type
2	13.45	6.47	11.77
3	13.45	6.47	11.77
4	13.45	6.47	11.77
5	13.45	6.47	11.77
6	12.73	6.47	11.86
7	12.73	6.47	11.86
8	9.54	6.47	11.00
9	9.54	6.47	11.00
10	7.15	6.25	6.05
11	7.15	6.25	6.05
12	6.96	4.70	8.85
13	6.96	4.70	8.85
14	5.35	4.33	6.42
15	5.35	4.33	6.42
16	5.16	4.21	5.01
17	5.16	4.21	5.01
18	5.16	3.92	5.01
19	5.16	3.92	5.01
20	5.16	3.87	5.01
21	5.16	3.87	5.01
22	5.16	3.28	5.01
23	5.16	3.28	5.01
24	5.16	3.17	5.01
25	5.16	3.17	5.01
NA	8.61	5.05	11.10

612

613   Appendix C) **STC**

C) Echo size within STC range:

$$P_{r_{min|stc,dBm}} = P_{r_{min}} - 40 \, log_{10}(distance/STC_{dist})$$

$$P_{r_{min|stc,W}} = P_{r_{min,W}} \cdot \frac{STC_{dist}^4}{distance^4}$$

D) Minimal RCS:

$$RCS_{min} = \frac{P_{r_{min,W}} \cdot STC_{dist}^4 \cdot (4 \cdot \pi)^3}{P_{t,W} \cdot G_0^2 \cdot \lambda^2}$$

A) Threshold:

$$P_{r_{min,dBm}} = 10 \cdot log_{10}(\frac{P_{r_{min,W}}}{1_{mW}})$$

B) STC_{dist} [m]

Received energy [dB]
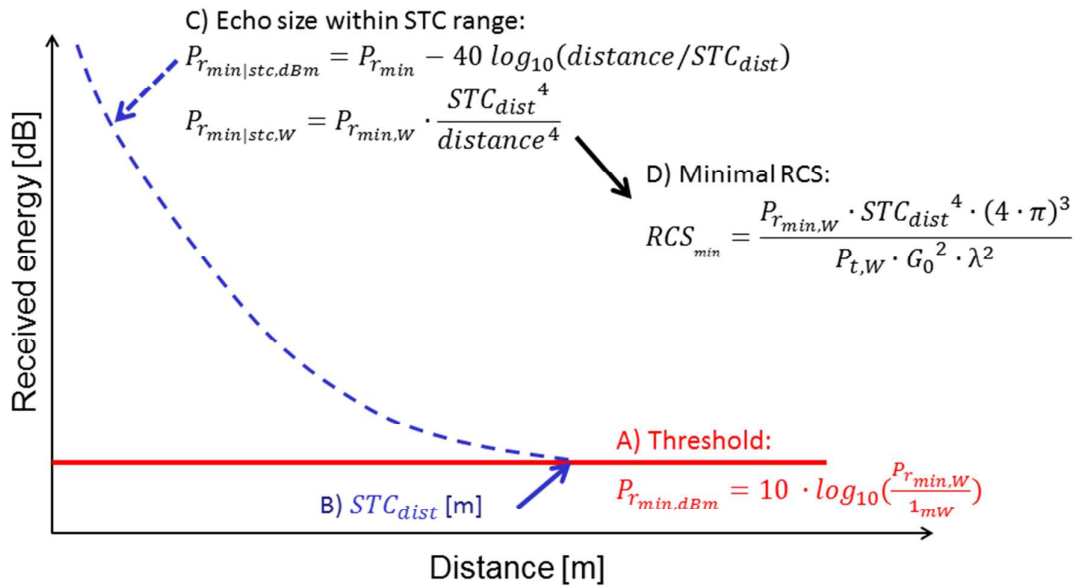
Distance [m]

614

615   Figure S1: Calculation of STC filter. A given detection threshold $\boldsymbol{P_{r_{min,dBm}}}$ (A) and a given $\boldsymbol{STC}$ (B), set a

616   distance-dependent echo size for detection (C, see Eq. 1). We obtain a RCS_{min} independent on the

617   distance within the STC-range, using the radar equation $RCS = \frac{P_r \cdot (4 \cdot \pi)^3 \cdot distance^4}{P_t \cdot G_0^2 \cdot \lambda^2}$, and replacing P_r by

618     $P_{r_{min|stc,W}}$. Within the STC, all echoes with echo size smaller than $\boldsymbol{P_{r_{min,dBm}}}$ (dashed blue line) have an

619   RCS smaller than RCS_{min} and are not detected, or removed post-hoc from the dataset.

620

621

29

622   Appendix D) **Monitored volume**

623   **Table A3**: Maximal detection distance D_{max} and effective beam area (and volume) depends on the sensitivity
624   settings (threshold $P_{r_{min,dBm}}$ and STC) assuming a typical object size of 15cm-diameter, transmitted power P_t
625   of 20 kW, and the antenna diagram provided by the manufacturer.

$P_{r_{min,dBm}}$	STC_{dist}	5 cm object diameter			15 cm object diameter		
		D_{max}	Total area	Total volume	D_{max}	Total area	Total volume
-93	300	765	111363	14614499	1361	350717	79758565
-90	300	636	77277	8506902	1137	245045	46913895
-87	300	527	53265	4897791	949	170624	27487956
-83	300	408	31613	2244713	744	105342	13462289
-93	500	765	102762	13016262	1361	336261	76233935
-90	500	636	67894	6910189	1137	233834	44451094
-87	500	527	40314	2974657	949	161713	25678177
-83	500	0	0	0	744	97073	11949402

626

627   Appendix E) **Influence of site identity on the RCS distributions**

628   Using 0.90-quantile of the RCS distribution, for Passerines only and finite WBF:

```
629    >lme1 = lme(ObjDiam_cm ~ wff_2Hz.of, random= ~ 1|campaignID.f, data=t.RCS,
630    control=list(maxIter = 100))
631    >summary(lme1)
632    Linear mixed-effects model fit by REML
633
634    Random effects:
635     Formula: ~1 | campaignID.f
636            (Intercept)  Residual
637    StdDev:   0.2230263 0.7332045
638
639    Fixed effects: ObjDiam_cm ~ wff_2Hz.of
640                     Value   Std.Error  DF   t-value  p-value
641    (Intercept)    4.546565 0.07850654 150   57.91321  0.0000
642    wff_2Hz.of.L  -2.342268 0.18330112 150  -12.77825  0.0000
643
```

644   The between-site variance (0.22 ± 0.73) is about 20 times smaller than the averaged site value

645   (Intercept 4.55 ± 0.08) and 10 times smaller than the decrease in RCS per two-Hertz (-2.34 ± 0.18)

646

647   Figure S3: Between site variance of the square-root RCS corrected for the wingbeat frequency

648   (sample size indicated on top).

649   Appendix F) **R-Functions**

650   funMinRCS

```
651    #*-**-**-**-**-**-**-**-**-**-**-**-**-**-**-**-**-**-**-**-**-**-**-**-**-*#
652    # original function snippet from Dominik Kleger, SwissBird Radar
653    TS = -93 # dBm as for Pr_min
654    Hmax = 300 # m as for STCdist
655    Psend = 22 # kW as for Pt
656    Again = 20 # dBi as for G0
657    funMinRCS <- function(TS=numeric(), Hmax=numeric(), Psend=numeric(), Again=numeric()){
658      min_rcs  <-  (10^(TS/10)  *  10^-3  *  Hmax^4  *  (4*pi)^3)/((Psend*10^3)  *  (10^(Again/10))^2  *
659    (3*10^8/(9.4*10^9))^2)
660      out <- min_rcs
661    }
662
663    funMTRfactor
664    #*-**-**-**-**-**-**-**-**-**-**-**-**-**-**-**-**-**-**-**-**-**-**-**-**-*#
665    # original function snippet from Dominik Kleger, SwissBird Radar
666    funMTRfactor = function(height, # distance of the object [m]
667                            objectDiameter, # object diameter in cm (sphere)
668                      waveguideAttenuation,  #  Attenuation  of  the  transmitted  and  received  power  by  the
669    waveguide [dB]
670                            stc_level, # min dBm value possible for a given height, as for Pr_min_stc
671                            Psend # in kW transmit power as for Pt
672    ){
673
674      # transform from kW to W
675      transmitPower = Psend * 1000
676      # compute back to radar cross-section in m^2 assuming spherical shape
677      rcs =  pi*(objectDiameter/100)^2/4
678
679      # MR1 specific parameters
680      lut_phi_table = seq(0,90,5) # antenna diagram angle in Grad
681      # diagram for "20dBiMR1"
682      lut_lev_table = c(20, 19.5, 17, 10, 6, 0, -3, -10, -13, -17, -20, -20, -19, -19, -23, -30, -21, -25, -30)
683       # antenna diagram Gain in dBi
684
685      #- using flatten spline at phi=0
686      xout <- unique(c(rev(seq(0, 90, 0.1)*-1), seq(0, 90, 0.1))) # use "unique" to avoid duplicated "0"
687      int_res = spline(x = c(rev(lut_phi_table*(-1)),lut_phi_table), y = c(rev(lut_lev_table), lut_lev_table),
688       xout = xout) # interpolate antenna diagram table
689      #  plot(int_res$x,  int_res$y, ylab="level", xlab="phi", xlim=c(-100,100), col="green", type="l")
690      #  points(lut_phi_table, lut_lev_table)
691      #  abline(v=90)
692      lut_lev = int_res$y[which(int_res$x >= 0)]
693      lut_phi = int_res$x[which(int_res$x >= 0)]
694
695      lut_lev_norm = lut_lev-lut_lev[1]
696      antennaGain = 10^((lut_lev[1]-waveguideAttenuation)/10)
697      f = 9.4e9 # electromagnetic wave frequency [Hz] or 9.4 GHz
698      c = 3e8 # light speed
699      # --> waveLength = c/f (see below in formula gainSTC)
700
701      # =======================================================
702      receiveLevelSTC = stc_level # alternatively use max(TS-40*log10(height/Hmax),  TS)
703      receivePowerSTC = 10^(receiveLevelSTC/10)*1e-3
704      gainSTC = sqrt(  (rcs*transmitPower*antennaGain^2*(c/f)^2) / ((4*pi)^3*height^4*receivePowerSTC)  )
705      levelSTC = -10*log10(gainSTC)
```

```
706    # values smaller than smallest antenna gain value -> set to value slightly higher than smallest antenna
707     gain value
708    index <- which(levelSTC <= lut_lev_norm[length(lut_lev_norm)])
709    levelSTC[index] = lut_lev_norm[length(lut_lev_norm)] + 0.1
710    # values bigger than biggest antenna gain value -> set value to zero
711    index <- which(levelSTC >= lut_lev_norm[1])
712    levelSTC[index] = 0
713
714    # compute phiSTC
715    phiSTC <- lapply(levelSTC, FUN=function(x){phiSTC = lut_phi[length(lut_lev_norm[lut_lev_norm > x])]})
716    index <- which(levelSTC >= 0)
717    phiSTC[index] <- 0
718    index <- which(phiSTC < 0)
719    phiSTC[index] <- 0
720    phiSTC <- unlist(phiSTC)
721
722    # get half-range
723    halfRangeSTC = height*tan(phiSTC/180*pi) # convert to m
724    # get full horizontal distance
725    RangeSTC = 2*halfRangeSTC # m
726    # get MTR-factor
727    MTRFactor = 1000*(1/RangeSTC) # convert to "targets per meter" and then to "targets per km"
728    MTRFactor[!is.finite(MTRFactor)] <- 0
729    # =================================================
730
731    return( data.frame("mtrf"=MTRFactor, "RangeSTC"=RangeSTC, "halfRangeSTC"=halfRangeSTC) )
732  }
733  # end function body
```